JACS
JOURNAL OF THE AMERICAN CHEMICAL SOCIETY
Article
pubs.acs.org/JACS

Accumulation of Multiple Oxidative Equivalents at a Single Site by Cross-Surface Electron Transfer on TiO_2

Wenjing Song,[†] Akitaka Ito,[†,‡] Robert A. Binstead, Kenneth Hanson, Hanlin Luo, M. Kyle Brennaman, Javier J. Concepcion, and Thomas J. Meyer*

Department of Chemistry, University of North Carolina at Chapel Hill, Chapel Hill, North Carolina 27599-3290, United States

Supporting Information

ABSTRACT: The photodriven accumulation of two oxidative equivalents at a single site was investigated on TiO_2 coloaded with a ruthenium polypyridyl chromophore $[Ru(bpy)_2((4,4'\text{-}(OH)_2PO)_2bpy)]^{2+}$ ($Ru^{II}P^{2+}$, bpy = 2,2′-bipyridine, $((OH)_2PO)_2$-bpy = 2,2′-bipyridine-4,4′-diyldiphosphonic acid) and a water oxidation catalyst $[Ru(Mebimpy)\ ((4,4'\text{-}(OH)_2PO{-}CH_2)_2bpy)(OH_2)]^{2+}$ ($Ru^{II}OH_2^{2+}$, Mebimpy = 2,6-bis(1-methylbenzimidazol-2-yl)pyridine, $(4,4'\text{-}(OH)_2PO{-}CH_2)_2bpy$) = 4,4′-bis-methlylenephosphonato-2,2′-bipyridine). Electron injection from the metal-to-ligand charge transfer (MLCT) excited state of $-Ru^{II}P^{2+}$ ($-Ru^{II}P^{2+}$*) to give $-Ru^{III}P^{3+}$ and $TiO_2(e^-)$ was followed by rapid (<20 ns) nearest-neighbor $-Ru^{II}OH_2^{2+}$ to $-Ru^{III}P^{3+}$ electron transfer. On surfaces containing both $-Ru^{II}P^{2+}$ and $-Ru^{III}OH_2^{3+}$ (or $-Ru^{III}OH^{2+}$), $-Ru^{II}OH_2^{2+}$ was formed by random migration of the injected electron inside the TiO_2 nanoparticle and recombination with the preoxidized catalyst, followed by relatively slow (μs-ms) non-nearest neighbor cross-surface electron transfer from $-Ru^{II}OH_2^{2+}$ to $-Ru^{III}P^{3+}$. Steady state illumination of coloaded TiO_2 photoanodes in a dye sensitized photoelectrosynthesis cell (DSPEC) configuration resulted in the buildup of $-Ru^{III}P^{3+}$, $-Ru^{III}OH^{2+}$, and $-Ru^{IV}{=}O^{2+}$, with $-Ru^{IV}{=}O^{2+}$ formation favored at high chromophore to catalyst ratios.

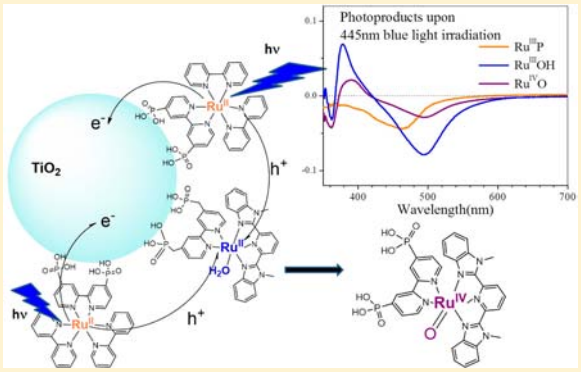

INTRODUCTION

A key element in natural and artificial photosynthesis is integrating components for solar photon harvesting, energy/electron transfer relays, and catalytic centers for water oxidation and water or CO_2 reduction in designed structures.[1−7] A number of strategies for combining chromophore and catalyst have been explored in dye-sensitized photoelectrosynthesis cells (DSPECs) for solar fuel production. In molecular assemblies where chromophores and catalysts are chemically linked,[8−10] self-assembled by layering strategies,[11] or introduced as supramolecular/polymer/peptide subunits,[12] the directionality of energy and electron transfer can be controlled by free energy gradients and through-space or through-bond orbital pathways.[13−16] In configurations with chromophore and catalyst coloaded on metal oxide semiconductor surfaces,[17−19] or confined in adsorbed films,[20] catalyst activation is mediated by electron transfer between adjacent molecules.[21,22]

A major challenge in DSPEC applications arises from the requirement for more than one excitation/electron transfer cycle to accumulate multiple redox equivalents at catalyst sites for solar fuel half reactions.[3,23] For efficient DSPECs, catalyst activation and catalytic reaction kinetics need to match or exceed solar photon flux. In DSPECs for water oxidation, accumulation of oxidative equivalents has been demonstrated indirectly by O_2 production and electrochemical characterization.[24−31] However, most dynamics studies have been limited to single photon-induced electron/hole transfer events.[17−19,32,33] Only a few reports are available describing the buildup and use of multiple redox equivalents in model systems.[8,9,34,35]

We have reported intramolecular electron transfer dynamics following excitation and electron injection in two bimetallic Ru^{II} assemblies. In these assemblies, excitation at the chromophore is followed by electron injection and intra-assembly electron transfer: $TiO_2\text{-}[Ru^{II}{-}Ru^{II}{-}OH_2]^{4+} \xrightarrow{h\nu} TiO_2(e^-){-}[Ru^{III}{-}Ru^{II}{-}OH_2]^{5+}$ and $TiO_2(e^-){-}[Ru^{III}{-}Ru^{II}{-}OH_2]^{5+} \rightarrow TiO_2(e^-){-}[Ru^{II}{-}Ru^{III}{-}OH_2]^{5+}$ which occurs on the subnanosecond time scale. These sequential events initiate the process of accumulation of oxidative equivalents at the remote catalyst in competition with back electron transfer, $TiO_2(e^-){-}[Ru^{II}{-}Ru^{III}{-}OH_2]^{5+} \rightarrow TiO_2{-}[Ru^{II}{-}Ru^{II}{-}OH_2]^{4+}$.[9,10]

Here we report the results of an investigation of cross-surface electron transfer on TiO_2 surfaces coloaded with a chromophore ($Ru^{II}P^{2+}$), and a water oxidation catalyst ($Ru^{II}OH_2^{2+}$). Structures are shown in Figure 1. On these surfaces, transient absorption measurements provide evidence for excitation and rapid injection by $TiO_2{-}Ru^{II}P^{2+}$* to give

Received: April 1, 2013
Published: July 12, 2013

   dx.doi.org/10.1021/ja4032538 | J. Am. Chem. Soc. 2013, 135, 11587−11594

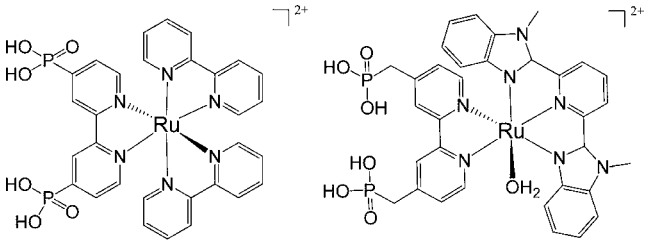

Figure 1. Structures of $Ru^{II}P^{2+}$ and $Ru^{II}OH_2^{2+}$.

$TiO_2(e^-)$–$Ru^{III}P^{3+}$. Injection is followed by rapid cross-surface oxidation of nearest neighbor $-Ru^{II}OH_2^{2+}$ sites to give $-Ru^{III}OH_2^{3+}$ or $-Ru^{III}OH^{2+}$ depending on pH. The use of cross-surface electron transfer to build up the active form of the catalyst, $-Ru^{IV}{=}O^{2+}$, is significantly inhibited by back electron transfer to preformed $-Ru^{III}OH_2^{3+}$ or $-Ru^{III}OH^{2+}$. Under steady state irradiation conditions, comparable to the solar photon flux, both $-Ru^{III}OH^{2+}$ and $-Ru^{IV}{=}O^{2+}$ build up on the semiconductor surface in pH 4.8 acetate buffer, with $-Ru^{III}OH^{2+}$ as the dominant species.

EXPERIMENTAL SECTION

Materials. Aqueous solutions were prepared from water purified by a Millipore Milli-Q Synthesis A10 purification system. Lithium perchlorate (99.999% trace metal basis), 70% perchloric acid (99.999%), lithium acetate (99.99%), titanium isopropoxide, and isopropanol were used as received from Sigma-Aldrich. Methanol and ethanol were obtained from Fisher Scientific. $[Ru(bpy)_2((4,4'\text{-}(OH)_2PO)_2bpy)]Cl_2$ ($Ru^{II}P^{2+}$, bpy = 2,2′-bipyridine, $((OH)_2PO)_2$-bpy = (2,2′-bipyridine-4,4′-diyldiphosphonic acid) and $[Ru(Mebimpy)((4,4'\text{-}(OH)_2PO{-}CH_2)_2bpy)(OH_2)](PF_6)_2$ ($Ru^{II}OH_2^{2+}$, Mebimpy = 2,6-bis(1-methylbenzimidazol-2-yl)pyridine, $(4,4'\text{-}(OH)_2PO{-}CH_2)_2$bpy, bpy = 4,4'-bis-methylenephosphonato-2,2′-bipyridine) were synthesized according to previously published procedures.[36,37]

Anatase TiO_2 (15–20 nm nanoparticles) or ZrO_2 (10–15 nm nanoparticles) films (11 mm × 20 mm, thickness ~ 6 ± 1 μm) on top of 11 mm × 70 mm FTO (fluorine-doped SnO_2, sheet resistance 15 Ω, Hartford Glass Co. Inc.) slides were prepared according to a reported literature procedure[9,38] The thickness of TiO_2 for steady state photoelectrolysis was reduced to ~3 μm in order to obtain more reliable absorbance spectral changes in the UV region. TiO_2/FTO photoanodes were sensitized by soaking in a 50–100 μM $Ru^{II}P^{2+}$ methanol solution, followed by a 50–100 μM $Ru^{II}OH_2^{2+}$ methanol solution. Relative surface coverage was controlled by loading times in the two solutions. Derivatized TiO_2 slides were immersed in electrolytes (0.1 M $HClO_4$ or dilute lithium acetate/acetic acid buffer) for 8–12 h before electrochemical or spectroscopic measurements. Molar absorptivity difference spectra between each oxidation state were obtained on TiO_2 by controlled potential electrolysis. In experiments with TiO_2 cosensitized with $Ru^{II}P^{2+}$ and $Ru^{III}OH_2^{3+}$/$Ru^{III}OH^{2+}$, the latter was generated by controlled potential electrolysis at 1.0 V vs NHE with 5 μM $Fe(bpy)_3^{2+}$ in the external solution as a redox mediator (E = 1.02 V vs NHE for the $Fe(bpy)_3^{3+/2+}$ couple). Surface coverages of each complex (Γ in mol cm^{-2}) were determined from Beer's Law with absorbance measurements at two different wavelengths using the molar absorptivities shown in Figure S1 in the Supporting Information.

Measurements. A customized three-arm photoelectrochemical cell was employed in the electrochemical and spectroelectrochemical measurements. The arm for the photoanode was a 10 mm path length Pyrex cuvette. A platinum wire was used as the cathode and Ag/AgCl as the reference electrode. The photoanode was inserted at a 45° angle into a homemade Teflon seat located in the cuvette part of the cell. All experiments were carried out under argon at (22 ± 2) °C unless otherwise specified. A CH Instruments model 601D potentiostat was employed for electrochemical characterization. UV–visible measurements were conducted on an Agilent Cary 50 UV–vis spectrophotometer.

Transient absorption (TA) measurements were carried out by inserting derivatized TiO_2 films at a 45° angle into a standard 10 mm path length square Pyrex cuvette containing electrolyte. The top of the cuvette was fit with an O-ring seal with a Kontes valve inlet to allow the contents to be purged with Argon. The experiments were performed by using nanosecond laser pulses produced by a Spectra-Physics Quanta-Ray Lab-170 Nd:YAG laser combined with a VersaScan OPO (5–7 ns, operated at 1 Hz, beam diameter 1 cm) integrated into a commercially available Edinburgh LP 920 laser flash photolysis spectrometer system. A white light probe pulse was generated by a pulsed 450 W Xe lamp. The probe light was passed through a 400 nm long pass filter before reaching the sample to avoid direct band gap excitation of TiO_2, then detected by a photomultiplier tube (Hamamatsu R928), or by a gated CCD (Princeton Instruments, PI-MAX3, gate width 10 ns, bandwidth 2.05 nm). Appropriate color filters were placed before the detector to reject unwanted scattered light. Single wavelength kinetic data were averaged over 50–100 laser shots.

Illumination for steady state photoelectrolysis was provided by a Lumencor spectral light engine (λ_{max} = 445 nm, 20 nm bandwidth, output ~ 1.7–83 mW). The light source was integrated with a Newport optical fiber and a focusing/imaging beam probe. The irradiation beam diameter was ~ 10 mm. Spectro-photoelectrochemical measurements were performed by combining the light source, CH Instruments 601D potentiostat, and Cary 50 UV–vis spectrophotometer.

Data Analysis. The transient absorption and steady state photolysis data were deconvoluted by Beer's law and converted to changes in concentration of various species. Dynamics and spectral data were modeled in Origin 8.5. For spectral modeling, a method for the standard addition of known spectra, written in the C programming language, was implemented in Origin's error minimization routine. Singular Value Deconvolution for the absorption time change data was performed with SPECFIT/32 software (Spectrum Software Associates).

RESULTS AND DISCUSSION

Electrochemistry and Spectroelectrochemistry. Electrochemical measurements on TiO_2 electrodes, coderivatized with $Ru^{II}P^{2+}$ and $Ru^{II}OH_2^{2+}$, were performed in 0.1 M $HClO_4$ or lithium acetate/acetic acid buffer with 0.1 M $LiClO_4$ (Figure S2). The redox potentials for oxidation of the surface-bound complexes fall within the band gap of TiO_2. Their oxidized forms are accessed indirectly by cross-surface electron transfer initiated by complexes adjacent to the underlying, conducting FTO electrode.[39–41] In cyclic voltammograms, a reversible $-Ru^{III}P^{3+}/-Ru^{II}P^{2+}$ wave appeared at $E_{1/2}$ = 1.32 ± 0.01 V vs NHE and was pH independent. The catalyst couples were pH dependent: for the $-Ru^{III}OH_2^{3+}/-Ru^{II}OH_2^{2+}$ couple, $E_{1/2}$ = 0.90 V (pH 1); and $E_{1/2}$ = 0.71 V for the $-Ru^{III}OH^{2+}/-Ru^{II}OH_2^{2+}$ couple at pH 4.5. The pH dependence is due to the proton coupled electron transfer (PCET) nature of the couple with $pK_{a,1}$ = 2.5 for $Ru^{III}OH_2^{3+}$.[42] Neither $-Ru^{IV}{=}O^{2+}$ nor $-Ru^{V}(O)^{3+}$ was observed due to slow cross-surface electron transfer on TiO_2.[39,40,43] On conductive *nano*ITO electrodes, at pH 1, the $-Ru^{IV}OH^{3+}/-Ru^{III}OH_2^{3+}$ couple was observed at $E_{1/2}$ = 1.26 V, and at pH 5 the $-Ru^{IV}{=}O^{2+}/-Ru^{III}OH^{2+}$ couple appeared at 1.0 V vs NHE (Table S1).[42,44,45] These results show that oxidation of $-Ru^{II}OH_2^{2+}$ by $-Ru^{III}P^{3+}$ on TiO_2 to give $-Ru^{III}OH_2^{3+}$, $-Ru^{III}OH^{2+}$, or $-Ru^{IV}{=}O^{2+}$ is thermodynamically favored.

dx.doi.org/10.1021/ja4032538 | J. Am. Chem. Soc. 2013, 135, 11587–11594

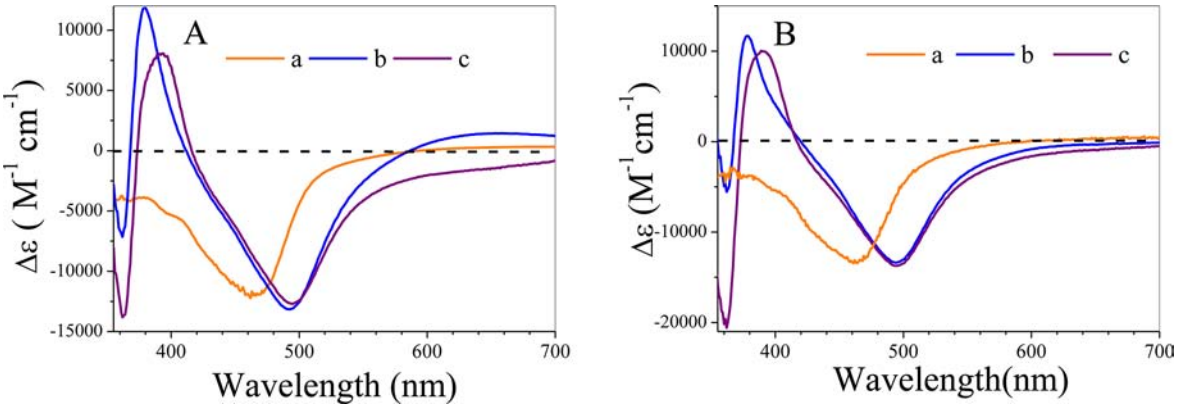

Figure 2. Molar absorptivity difference spectra between (a) TiO_2–$Ru^{III}P^{3+}$ and TiO_2–$Ru^{II}P^{2+}$, (b) TiO_2–$Ru^{III}OH_2^{3+}$ (or $Ru^{III}OH^{2+}$) and TiO_2–$Ru^{II}OH_2^{2+}$, and (c) TiO_2–$Ru^{IV}OH^{3+}$ (or $Ru^{IV}{=}O^{2+}$) and TiO_2–$Ru^{II}OH_2^{2+}$. (A) in 0.1 M $HClO_4$; (B) in pH 4.8 LiOAc/HOAc buffer with 0.1 M $LiClO_4$.

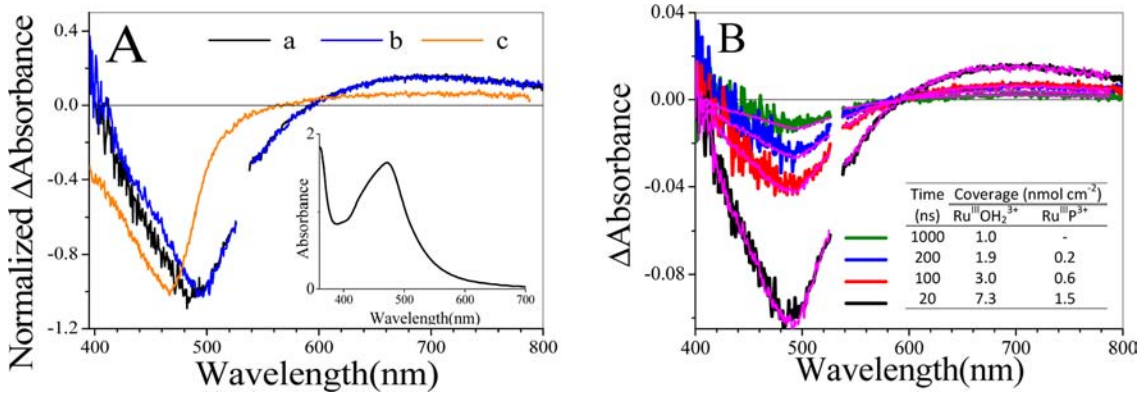

Figure 3. (A) Transient absorption difference spectra on (a) TiO_2–$Ru^{II}P^{2+}$/$Ru^{II}OH_2^{2+}$ (8×10^{-8} mol cm^{-2}/4×10^{-8} mol cm^{-2}), (b) TiO_2–$Ru^{II}OH_2^{2+}$ (5.7×10^{-8} mol cm^{-2}), and (c) TiO_2–$Ru^{II}P^{2+}$ (4.3×10^{-8} mol cm^{-2}) acquired 20 ns following 532 nm laser excitation in 0.1 M $HClO_4$ at room temperature. Insert: absorption spectrum of sample (a). (B) Transient absorption spectra of TiO_2–$Ru^{II}P^{2+}$/$Ru^{II}OH_2^{2+}$ (from panel A) at various times after photo excitation. Overlaid are the best spectral modeling fits (magenta) to the amount of $-Ru^{III}P^{3+}$ and $-Ru^{III}OH_2^{3+}$. Inset Table: calculated amounts of $-Ru^{III}P^{3+}$ and $-Ru^{III}OH_2^{3+}$ from the spectra.

Spectral changes for oxidation of TiO_2–$Ru^{II}P^{2+}$ to TiO_2–$Ru^{III}P^{3+}$, and TiO_2–$Ru^{II}OH_2^{2+}$ to TiO_2–$Ru^{III}OH_2^{3+}$, and further to TiO_2–$Ru^{IV}OH^{3+}$ in 0.1 M $HClO_4$ are shown in Figure 2A. The most distinguishing difference between the spectra of $-Ru^{III}OH_2^{3+}$ and $-Ru^{IV}OH^{3+}$ is in the UV region (360–420 nm, Figure S3). A similar trend was observed for spectral changes obtained in pH 4.8 buffer (Figure 2B), where $-Ru^{III}OH^{2+}$ and $-Ru^{IV}{=}O^{2+}$ were generated. These spectra were used in calculating the photoproduct distribution on TiO_2.

Photoinduced, Cross-Surface Oxidation of $-Ru^{II}OH_2^{2+}$ to $-Ru^{III}OH_2^{3+}$. Photoinduced events on coloaded TiO_2 were monitored by nanosecond transient absorption. A transient difference spectrum obtained 20 ns following 532 nm excitation of TiO_2–$Ru^{II}P^{2+}$/$Ru^{II}OH_2^{2+}$ (8×10^{-8} mol cm^{-2}/4×10^{-8} mol cm^{-2}) in 0.1 M $HClO_4$ is shown in Figure 3. Also shown are the transient difference spectra for TiO_2–$Ru^{II}P^{2+}$ and TiO_2–$Ru^{II}OH_2^{2+}$ obtained independently by 532 nm excitation.

Spectral deconvolution of the transient absorption spectrum after excitation of cosensitized TiO_2 revealed the formation of 1.5 nmol cm^{-2} $-Ru^{III}P^{3+}$ and 7.3 nmol cm^{-2} $-Ru^{III}OH_2^{3+}$; that is, ~83% of the oxidative equivalents (holes) were on the catalyst. From the relative light absorptions by TiO_2–$Ru^{II}P^{2+}$ and TiO_2–$Ru^{II}OH_2^{2+}$ at the excitation wavelength (Figure S4), and their independently measured electron injection efficiencies ($\Phi_{inj,\ RuP} = 1.0$; $\Phi_{inj,\ RuOH2} = 0.25$, eq 1a and 1b), direct electron injection was responsible for ~38% of the oxidative equivalents at the catalyst site (eq 2). In eq 2, Γ is the surface coverage, I_a is the absorbed light at the excitation wavelength, and Φ_{inj} is the electron injection yield.

$$TiO_2\text{–}Ru^{II}P^{2+} \xrightarrow{h\nu} TiO_2(e^-)\text{–}Ru^{III}P^{3+} \quad (1a)$$

$$TiO_2\text{–}Ru^{II}OH_2^{2+} \xrightarrow{h\nu} TiO_2(e^-)\text{–}Ru^{III}OH_2^{3+} \quad (1b)$$

$$\Gamma(Ru^{III}OH_2^{3+})/\Gamma(Ru^{III}P^{3+}) = (I_{a,RuOH2}/I_{a,RuP})(\Phi_{inj,RuOH2}/\Phi_{inj,RuP}) \quad (2)$$

Based on these calculations, ~73% of the oxidative equivalents at TiO_2–$Ru^{III}OH_2^{3+}$ following laser flash photolysis were generated by cross-surface hole transfer from TiO_2–$Ru^{III}P^{3+}$ to TiO_2–$Ru^{II}OH_2^{2+}$ (eq 3) within 20 ns. On a fully covered TiO_2 surface, each $-Ru^{II}OH_2^{2+}$ site has multiple $-Ru^{II}P^{2+}$ neighbors with center-to-center distances of ~1.4 nm.[46] Evidence for the importance of close contact for rapid electron transfer comes from the observation that, on ~40% covered TiO_2, with a similar chromophore-to-catalyst ratio, 3.5×10^{-8}/1.7×10^{-8} mol cm^{-2}, the cross-surface electron transfer efficiency at 20 ns decreased to 14% (Figure S5). Under these

dx.doi.org/10.1021/ja4032538 | J. Am. Chem. Soc. 2013, 135, 11587–11594

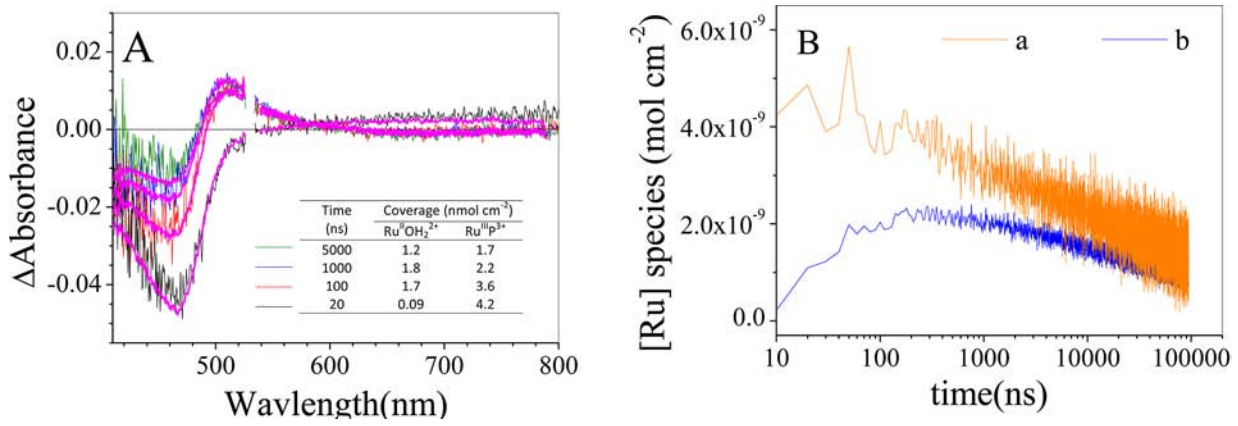

Figure 4. (A) Transient absorption difference spectra for TiO_2–$Ru^{II}P^{2+}$/$Ru^{III}OH_2^{3+}$ (8×10^{-8} mol cm^{-2}/4×10^{-8} mol cm^{-2}) at various times following 532 nm laser excitation in 0.1 M $HClO_4$. Overlaid are the best spectral fits (magenta) to the amount of –$Ru^{III}P^{3+}$ and –$Ru^{II}OH_2^{2+}$ formed (inset table). (B) Dynamics of –$Ru^{III}P^{3+}$ (a, orange) and –$Ru^{II}OH_2^{2+}$ (b, blue) from deconvoluted absorption–time traces at 460 and 490 nm. (Note: there could be some inconsistency in calculated surface coverage by modeling the spectra in panel A and by the deconvolution from two wavelengths in panel B.)

conditions, photoinduced events are dominated by electron injection and back electron transfer.

$$TiO_2(e^-)–Ru^{III}P^{3+},\ TiO_2–Ru^{II}OH_2^{2+} \rightarrow TiO_2(e^-)–Ru^{II}P^{2+},\ TiO_2–Ru^{III}OH_2^{3+} \quad (3)$$

Transient absorption spectral changes at various times following laser excitation at 532 nm are shown in Figure 3B. The inset table shows the calculated amounts of –$Ru^{III}P^{3+}$ and –$Ru^{III}OH_2^{3+}$ in nmol cm^{-2}. After 1 μs, nearly complete reduction of –$Ru^{III}P^{3+}$ to –$Ru^{II}P^{2+}$ was observed, while ~14% of the –$Ru^{III}OH_2^{3+}$ remained on the surface.[9,11,43] According to the results of earlier studies, back electron transfer to both –$Ru^{III}P^{3+}$ and –$Ru^{III}OH_2^{3+}$ under these conditions is rate limited by electron transport dynamics within the TiO_2 and occurs on similar time scales ($t_{1/2}$ ~ 0.3–0.5 μs).[9−11,43,47−49] The more rapid reappearance of –$Ru^{II}P^{2+}$ on the mixed surface was due to electron transfer from non-nearest neighbor –$Ru^{II}OH_2^{2+}$. Since 73% of the cross-surface electron transfer events occur within the first 20 ns under these experimental conditions, it is difficult to resolve the dynamics of the residual electron transfer events due to complications from back electron transfer.

Photoinduced Cross-Surface Oxidation of –$Ru^{III}OH_2^{3+}$ or –$Ru^{III}OH^{2+}$. Chemical or electrochemical oxidation of $Ru^{II}OH_2^{2+}$ by sequential proton coupled electron transfer gives $Ru^{IV}{=}O^{2+}$.[42] There is an extensive stoichiometric and catalytic oxidation chemistry of $Ru^{IV}{=}O^{2+}$ toward a variety of inorganic and organic functional groups.[50]

Photoproduction of –$Ru^{IV}OH^{3+}$ was first investigated on TiO_2 coloaded with –$Ru^{II}P^{2+}$:–$Ru^{III}OH_2^{3+}$ in 0.1 M $HClO_4$ by nanosecond transient absorption. As shown in Figure 2A, spectral changes accompanying oxidation of –$Ru^{III}OH_2^{3+}$ to –$Ru^{IV}OH^{3+}$ are small in the region 400–700 nm except for an ~3000 M^{-1} cm^{-1} decrease in absorptivity at 650 nm, an ~4000 M^{-1} cm^{-1} increase at 400 nm, and an ~8000 M^{-1} cm^{-1} decrease at 360 nm. On TiO_2–$Ru^{II}P^{2+}$/$Ru^{III}OH_2^{3+}$ (8×10^{-8} mol cm^{-2}/4×10^{-8} mol cm^{-2}), these features were difficult to discern in the transient spectra (Figure 4A) due to the low signal-to-noise level in the UV region. By contrast, the most distinct feature following 532 nm laser excitation is a positive absorption at 510 nm. The changes in the transient spectra with time were best fit to the generation of –$Ru^{III}P^{3+}$ and the formation of –$Ru^{II}OH_2^{2+}$ which is responsible for the positive feature from 500 to 550 nm. There was no evidence supporting rapid cross-surface oxidation of –$Ru^{III}OH_2^{3+}$ to –$Ru^{IV}OH^{3+}$. Instead, injected electrons diffuse randomly within TiO_2 and recombine with both –$Ru^{III}P^{3+}$ and –$Ru^{III}OH_2^{3+}$. The proposed sequence of events is shown in eqs 4 and 5. The loss of –$Ru^{III}P^{3+}$ and growth/decay of –$Ru^{II}OH_2^{2+}$ were deconvoluted from the absorption-time traces with the results shown in Figure 4B.

$$TiO_2(e^-)–Ru^{III}P^{3+},\ TiO_2–Ru^{III}OH_2^{3+} \rightarrow TiO_2–Ru^{II}P^{2+},\ TiO_2–Ru^{III}OH_2^{3+} \quad (4)$$

$$TiO_2(e^-)–Ru^{III}P^{3+}...TiO_2–Ru^{III}OH_2^{3+} \rightarrow TiO_2–Ru^{III}P^{3+}...TiO_2(e^-)–Ru^{III}OH_2^{3+} \rightarrow TiO_2–Ru^{III}P^{3+}...TiO_2–Ru^{II}OH_2^{2+} \quad (5)$$

$$TiO_2–Ru^{III}P^{3+}...TiO_2–Ru^{II}OH_2^{2+} \rightarrow TiO_2–Ru^{II}P^{2+}...TiO_2–Ru^{III}OH_2^{3+} \quad (6)$$

As shown in Figure 4B, past 10 μs, the concentrations of residual –$Ru^{III}P^{3+}$ and –$Ru^{II}OH_2^{2+}$ were close and decay with similar kinetics. The original state before excitation was recovered by cross-surface electron transfer (eq 6). However, in contrast to the <20 ns time scale for electron transfer between donor and acceptor in close contact, the event observed here required hundreds of microseconds to milliseconds to reach completion. This observation is similar to one made earlier on TiO_2 coloaded with the Z907 dye (*cis*-[Ru(dnb)(dcb)$(NCS)_2$], dnb is 4,4′-dinonyl-bpy; dcb is 4,4′-(COOH)2-bpy; bpy is 2,2′-bipyridine) and a Co(II) complex at 100:1 ratio. On this surface, multiple electron self-exchange events occurred between surface-bound dye molecules followed by oxidation of remote Co^{II} to Co^{III}.[17,18]

The remarkable difference in rates here arises from random migration of the injected electron within the TiO_2 nanoparticle and recombines with –$Ru^{III}OH_2^{3+}$ (eq 5) to form –$Ru^{II}OH_2^{2+}$ away from the electron injection site.[47,48,51] As illustrated in eqs 5 and 6, this increases the average distance between –$Ru^{II}OH_2^{2+}$ and –$Ru^{III}P^{3+}$, leading to slow cross-surface

dx.doi.org/10.1021/ja4032538 | J. Am. Chem. Soc. 2013, 135, 11587–11594

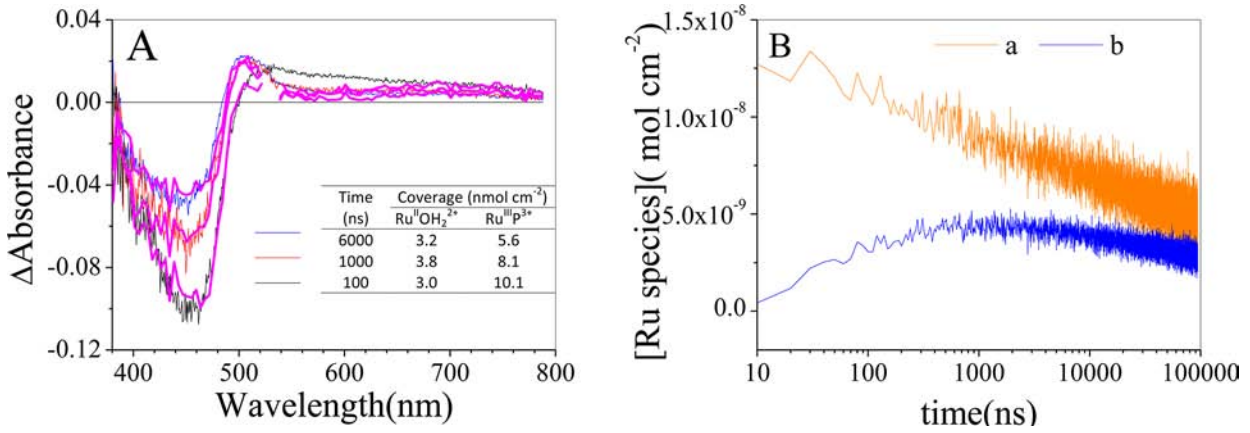

Figure 5. (A) Transient absorption difference spectra for TiO_2–$Ru^{II}P^{2+}$/$Ru^{III}OH^{2+}$ (1×10^{-7} mol cm^{-2}/3.2×10^{-8} mol cm^{-2}) at various times after 532 nm laser excitation in 10 mM pH 5 LiOAc/HOAc buffer with 0.1 M $LiClO_4$. Overlaid (magenta) are the best fits for the amounts of –$Ru^{III}P^{3+}$ and –$Ru^{II}OH_2^{2+}$ (inset table). (B) Dynamics of –$Ru^{III}P^{3+}$ (a, orange) and –$Ru^{II}OH_2^{2+}$ (b, blue) from deconvoluted absorption-time traces at 460 and 490 nm.

electron transfer. Long-range electron transfer is also mediated by multiple-step nearest-neighbor electron hopping events (–$Ru^{III}P^{3+}$, –$Ru^{II}P^{2+}$ → –$Ru^{II}P^{2+}$, –$Ru^{III}P^{3+}$) which may take up to a millisecond.

The kinetics of –$Ru^{II}OH_2^{2+}$ to –$Ru^{III}P^{3+}$ electron transfer (eq 6) was highly nonexponential. The decay of –$Ru^{II}OH_2^{2+}$ was fit to the stretched exponential function in eq 7, where A_0 is the initial value of –$Ru^{II}OH_2^{2+}$ (decay part Figure 4B, b), β is inversely related to the width of the underlying Lévy distribution of rate constants with $0 < \beta < 1$, and τ is the characteristic lifetime. The fit gives a characteristic lifetime of $\tau \sim 110$ μs and $\beta \sim 0.32$, These observations show that both nearest-neighbor oxidation of –$Ru^{II}OH_2^{2+}$ by –$Ru^{III}P^{3+}$ and electron diffusion in TiO_2 are more rapid than long-range, cross-surface electron transfer.

$$A_t = A_0\, e^{-(t/\tau)^{\beta}} \tag{7}$$

The absence of cross surface oxidation of –$Ru^{III}OH_2^{3+}$ to –$Ru^{IV}OH^{3+}$ at pH 1 is presumably due to the small thermodynamic driving force ($\Delta G^{\circ\prime} \sim -0.07$ eV for oxidation of –$Ru^{III}OH_2^{3+}$ to –$Ru^{IV}OH^{3+}$ by –$Ru^{III}P^{3+}$), and the inaccessibility of the high energy, protonated oxo, –$Ru^{IV}OH_2^{4+}$ form of the catalyst as an intermediate (eq 8).

$$\begin{aligned} &TiO_2(e^-) - Ru^{III}P^{3+},\ TiO_2 - Ru^{III}OH_2^{3+} \\ &\rightarrow TiO_2(e^-) - Ru^{II}P^{2+},\ TiO_2 - Ru^{IV}OH_2^{4+} \\ &\rightarrow TiO_2(e^-) - Ru^{II}P^{2+},\ TiO_2 - Ru^{IV}OH^{3+} + H^+ \end{aligned} \tag{8}$$

Photoinduced generation of Ru^{IV} is favored at higher pHs above $pK_{a,1}$ for –$Ru^{III}OH_2^{3+}$ based on previous electrochemical measurements. With the dominant form of the catalyst on the surface as –$Ru^{III}OH^{2+}$ at pH 5, $E_{1/2} = 1.1$ V for the $Ru^{IV}OH^{3+}$/$Ru^{III}OH^{2+}$ couple and $E_{1/2} = 1.0$ V for the $Ru^{IV}{=}O^{2+}$/$Ru^{III}OH^{2+}$ couple (Table S1).[42] –$Ru^{IV}{=}O^{2+}$ is accessible by both sequential electron transfer-proton transfer (ET-PT, eq 9a), or, by simultaneous electron–proton transfer with an added base (EPT, eq 9b).[42]

$$\begin{aligned} &TiO_2(e^-){-}Ru^{III}P^{3+},\ TiO_2{-}Ru^{III}OH^{2+} \\ &\rightarrow TiO_2(e^-){-}Ru^{II}P^{2+},\ TiO_2 - Ru^{IV}OH^{3+} \\ &\xrightarrow{-H^+} TiO_2(e^-){-}Ru^{II}P^{2+},\ TiO_2{-}Ru^{IV} = O^{2+} \end{aligned} \tag{9a}$$

$$\begin{aligned} &TiO_2(e^-){-}Ru^{III}P^{3+},\ TiO_2{-}Ru^{III}OH{\cdots}OAc^- \\ &\rightarrow TiO_2(e^-){-}Ru^{II}P^{2+},\ TiO_2{-}Ru^{IV}{=}O^{2+} + HOAc \end{aligned} \tag{9b}$$

With –$Ru^{III}OH^{2+}$ as the dominant form of the catalyst on the surface, cross-surface oxidative activation to –$Ru^{IV}{=}O^{2+}$ is in competition with rereduction of –$Ru^{III}OH^{2+}$ to –$Ru^{II}OH^{+}$ (eq 10a), which is less favored than reduction of –$Ru^{III}OH^{2+}$ to –$Ru^{II}OH_2^{2+}$ (eq 10b) by 0.4 eV at pH 5.[52]

$$\begin{aligned} &TiO_2(e^-){-}Ru^{III}OH^{2+} \\ &\rightarrow TiO_2{-}Ru^{II}OH^{+} \\ &\xrightarrow{+H^+} TiO_2{-}Ru^{II}OH_2^{2+} \end{aligned} \tag{10a}$$

$$TiO_2(e^-){-}Ru^{III}OH^{2+} + H^+ \rightarrow TiO_2{-}Ru^{II}OH_2^{2+} \tag{10b}$$

To explore the role of deprotonation of –$Ru^{III}OH_2^{3+}$, we performed transient absorption measurements in pH 5 acetate buffer. Spectral-time profiles on TiO_2 coloaded with a 3:1 ratio of $Ru^{II}P^{2+}$/$Ru^{III}OH^{2+}$ (1.0×10^{-7}/3.2×10^{-8} mol cm^{-2}) were qualitatively similar to those obtained at pH 1 with a positive absorption feature appearing at 510 nm due to recombination of $TiO_2(e^-)$ with preformed –$Ru^{III}OH^{2+}$ (Figure 5A). Although spectral modeling may indicate the presence of –$Ru^{IV}{=}O^{2+}$, the amount of –$Ru^{IV}{=}O^{2+}$ was too small to make significant contributions to the observed transient spectra. The spectra could also be modeled by –$Ru^{III}OH^{2+}$ and –$Ru^{III}P^{3+}$ without –$Ru^{IV}{=}O^{2+}$.

Figure 5B illustrates the dynamics of –$Ru^{III}P^{3+}$ and –$Ru^{II}OH_2^{2+}$ following laser excitation at 532 nm. During the first 1000 ns, ~4.2 nmol cm^{-2} –$Ru^{III}OH^{2+}$ underwent recombination with injected electrons to give –$Ru^{II}OH_2^{2+}$. Within the same time window, ~3 nmol cm^{-2} –$Ru^{III}P^{3+}$ either recombined with $TiO_2(e^-)$ or oxidized –$Ru^{III}OH^{2+}$ to –$Ru^{IV}{=}O^{2+}$. The kinetics for the ensuing decay of –$Ru^{II}OH_2^{2+}$, by cross-surface electron transfer from –$Ru^{II}OH_2^{2+}$ to –$Ru^{III}P^{3+}$, were fit to the stretched exponential function in eq 7 with τ =

dx.doi.org/10.1021/ja4032538 | J. Am. Chem. Soc. 2013, 135, 11587–11594

420 μs and β = 0.42. The τ and β values from this analysis varied significantly from sample to sample, depending on loading ratio and excitation fluence. Consequently, changes observed in these parameters could not be attributed solely to pH.

A summary of the proposed photoinduced events on coderivatized TiO_2 at pH ∼5 is shown in Scheme 1. The

Scheme 1. Photoinduced Events on a TiO_2 Surface Coloaded with $-Ru^{II}P^{2+}$ and $-Ru^{II}OH_2^{2+}$ at pH 5[a]

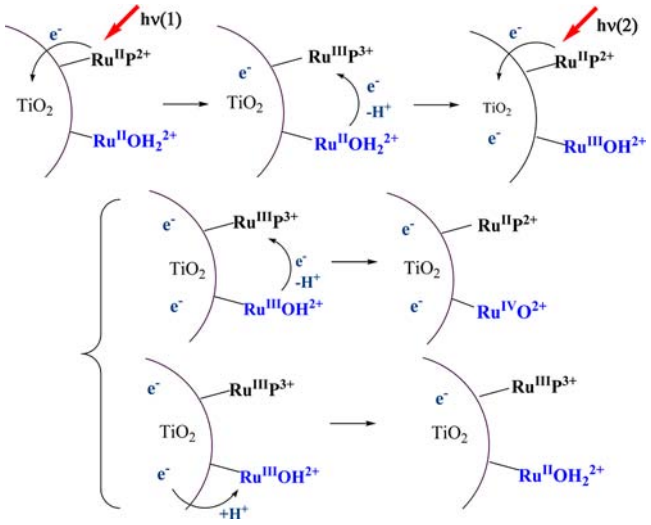

[a]Light absorption and electron injection by $-Ru^{II}OH_2^{2+}$ are not shown. Preliminary results on coloaded ZrO_2 (Figure S6 and S7) show that rate constants for cross-surface energy transfer from $-RuP^{2+}$* to $-Ru^{II}OH_2^{2+}$ ($-Ru^{II}P^{2+}$*, $-Ru^{II}OH_2^{2+} \rightarrow -Ru^{II}P^{2+}$, $-Ru^{II}OH_2^{2+}$*) and electron transfer from $-Ru^{II}P^{2+}$* to $-Ru^{III}OH_2^{2+}$ ($-Ru^{II}P^{2+}$*, $-Ru^{III}OH_2^{2+} \rightarrow -Ru^{III}P^{3+}$, $-Ru^{II}OH_2^{2+}$) are far slower than electron injection (20 fs to 200 ps[53]), and they are not included here.

scheme includes cross-surface oxidation of $-Ru^{III}OH^{2+}$ to $-Ru^{IV}{=}O^{2+}$. As discussed below, even though the evidence for $-Ru^{IV}{=}O^{2+}$ by the transient absorbance measurements is equivocal, there is evidence for photoinduced generation of $-Ru^{IV}{=}O^{2+}$ under steady state photolysis conditions.

Steady-State Accumulation of $-Ru^{IV}{=}O^{2+}$. Accumulation of multiple oxidative equivalents on the surface of TiO_2 as $-Ru^{IV}{=}O^{2+}$, $-Ru^{IV}{-}OH^{3+}$, or $-Ru^{V}{=}O^{2+}$ is an essential element in carrying out water splitting or organic oxidations in DSPEC configurations. Compared to DSSCs, which are inherently $1e^-/1$ photon devices, multiple excitation and generation of oxidative equivalents are required. In addition, the second excitation must occur within the lifetime of the initial photoproduct, before back electron transfer is complete.[8,34]

Given what is known about interfacial dynamics of $TiO_2(e^-){-}Ru^{III}P^{3+}$, with back electron transfer occurring on the microsecond to millisecond time scale,[52,54,55] buildup of even the second oxidative equivalent is challenging. Accumulating multiple oxidative equivalents must also overcome losses from relatively slow electron transport to the underlying collector electrode as well as back electron transfer to the surface-oxidized complex.

On mesoporous nanocrystalline TiO_2 films, ruthenium polypyridyl chromophores are excited 1−2 times per second under solar photon flux.[56,57] Given the requirement for multiple oxidative equivalents for half reactions like water oxidation, there is a clear advantage to couple multiple chromophores and excitation events to single-site catalysts activation.

Steady state photolysis under irradiation conditions comparable to the solar photon flux was investigated for coloaded TiO_2 in a DSPEC configuration under operating conditions in pH 4.8 acetate buffers. Table 1 summarizes the photoproducts

Table 1. Surface Coverage and (Photo)products in nmol cm^{-2} on TiO_2 Photoanodes under 8.3 mW 445 nm Irradiation in 20 mM pH 4.8 Acetate Buffer with 0.1 M $LiClO_4$

$-Ru^{II}P^{2+}/-Ru^{II}OH_2^{2+}$	bias vs NHE	$-Ru^{III}P^{3+}$	$-Ru^{III}OH^{2+}$	$-Ru^{IV}{=}O^{2+}$
32.2/17.9	0.2	1.8	14.3	0
51.2/8.0	0.2	3.3	6.5	1.5(2.1)[b]
28.0/9.5	0.9[a]	0.2	7.1	0
	0.9	3.2	7.9	1.6(2.1)[b]

[a]Controlled potential electrolysis without irradiation for ∼45 min. [b]$[-Ru^{IV}{=}O^{2+}]$ values obtained by spectral modeling shown in parentheses were higher than ($[-Ru^{II}OH_2^{2+}] - [-Ru^{III}OH^{2+}]$), and the latter value is used here.

with different $-Ru^{II}P^{2+}/-Ru^{II}OH_2^{2+}$ ratios. Photolysis was performed with a bias applied to the photoanode in order to extract the collected electrons to the FTO substrate. The net reaction in the cell is photo-oxidation of $-Ru^{II}P^{2+}$ and $-Ru^{II}OH_2^{2+}$, with reduction of protons to hydrogen at the cathode. The spectral changes observed under these conditions are shown in Figure 6.

At relatively low ratios of $-Ru^{II}P^{2+}$ to $-Ru^{II}OH_2^{2+}$ (Figure 6A and Table 1, row 1), with 0.2 V applied bias, photoinduced oxidation of $-Ru^{II}OH_2^{2+}$ was incomplete and formation of $-Ru^{IV}{=}O^{2+}$ was negligible. Increasing the $-Ru^{II}P^{2+}/-Ru^{II}OH_2^{2+}$ ratio to 6.4 resulted in spectral changes in the UV that provided clear evidence for the buildup of $-Ru^{IV}{=}O^{2+}$ (Figure 6B and Table 1, row 2). This can be seen in the mismatch from 350 to 420 nm with the spectrum modeled without including $-Ru^{IV}{=}O^{2+}$ (cyan, also note the enlarged figure in Figure S8A). Under these conditions, all $-Ru^{II}OH_2^{2+}$ was oxidized, with $-Ru^{III}OH^{2+}$ as the dominant product on the surface.

Based on the deconvoluted absorption spectrum, 70−86% of the light was absorbed by $-Ru^{II}P^{2+}$. This shows that the appearance of $-Ru^{III}OH^{2+}$ and $-Ru^{IV}{=}O^{2+}$ is largely due to cross-surface electron transfer events, not from excited state electron injection from the catalyst. The lower yield of $-Ru^{IV}{=}O^{2+}$ is also consistent with competition from back electron transfer to (photo)generated $-Ru^{III}OH^{2+}$. More steady state photoelectrolysis results can be found in the Supporting Information (Figure S8 and table S2).

Formation of $-Ru^{IV}{=}O^{2+}$ was also observed on surfaces with the catalyst present initially as $-Ru^{III}OH^{2+}$. $-Ru^{III}OH^{2+}$ was generated by controlled potential electrolysis of $-Ru^{II}OH_2^{2+}$ at 0.9 V vs NHE. Upon photolysis, only 23% of the preformed $-Ru^{III}OH^{2+}$ was further converted to $-Ru^{IV}{=}O^{2+}$ (Figure 6C and Table 1, row 3).

These analyses are of limited accuracy due to the uncertainties in the spectral modeling (see the Supporting Information, section VI and Figure S8). Additional complications may also appear from decomposition of $-Ru^{II}P^{2+}$ during photolysis or entry of the catalyst into the water oxidation cycle

dx.doi.org/10.1021/ja4032538 | J. Am. Chem. Soc. 2013, 135, 11587−11594

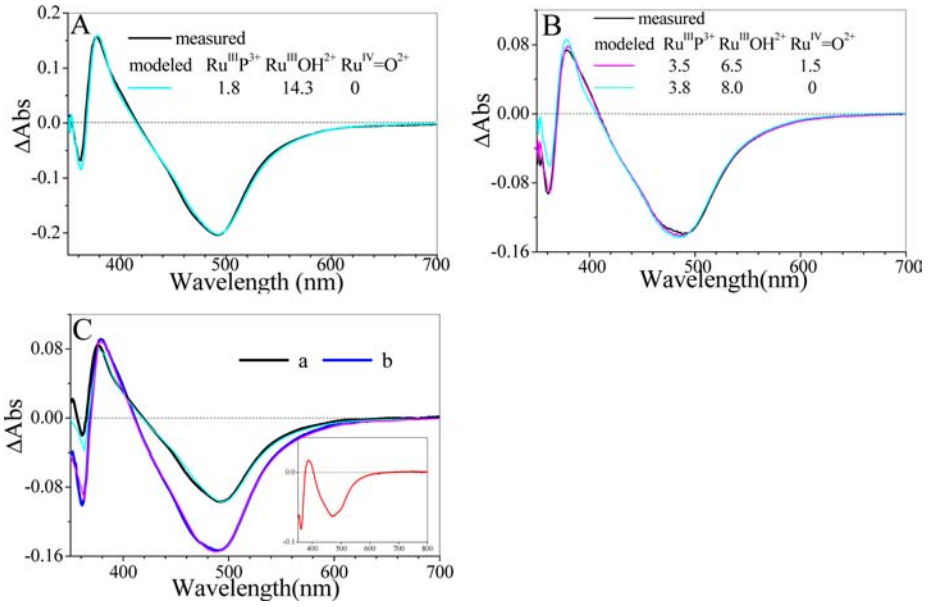

Figure 6. Spectral changes observed at coloaded TiO_2 photoanodes upon 445 nm (8.3 mW) irradiation for ~200−300 s (to approach photoequilibrium). Overlaid curves are spectral modeling results with (magenta) or without (cyan) $-Ru^{IV}{=}O^{2+}$. The calculated concentration of each species is shown in nmol cm^{-2}. (A) 3.2×10^{-8} mol cm^{-2} $-Ru^{II}P^{2+}$ and 1.8×10^{-8} mol cm^{-2} $-Ru^{II}OH_2{}^{2+}$, with 0.2 V applied bias to the photoanode; (B) 5.1×10^{-8} mol cm^{-2} $-Ru^{II}P^{2+}$ and 8.0×10^{-9} mol cm^{-2} $-Ru^{II}OH_2{}^{2+}$, with 0.2 V bias applied to the photoanode; (C) 2.8×10^{-8} mol cm^{-2} $-Ru^{II}P^{2+}$ and 9.5×10^{-9} mol cm^{-2} $-Ru^{II}OH_2{}^{2+}$: (a) after controlled potential electrolysis at 0.9 V vs NHE for ~45 min, (b) spectral change upon 300 s irradiation with bias held at 0.9 V, insert shows the difference, (b) − (a). The electrolyte was 20 mM pH 4.8 acetate buffer with 0.1 M $LiClO_4$.

with generation of $-Ru^{III}OOH^{2+}$ intermediate on the surface.[45,58] Nonetheless, spectral changes and the surface coverage dependence clearly support the buildup of the twice-oxidized catalyst $-Ru^{IV}{=}O^{2+}$ on the surface.

CONCLUSIONS

We have reported here the dynamics of cross surface electron transfer on TiO_2 coloaded with both chromophore ($Ru^{II}P^{2+}$) and catalyst ($Ru^{II}OH_2{}^{2+}$), and the stepwise accumulation of multiple oxidative equivalents at the water oxidation catalyst site as $-Ru^{IV}{=}O^{2+}$. Oxidation of the catalyst occurs by electron injection from $-Ru^{II}P^{2+}{*}$, and the following nearest neighbor cross-surface electron transfer from $-Ru^{II}OH_2{}^{2+}$ to $-Ru^{III}P^{3+}$ occurs on the <20 ns time scale. Following electron injection on surfaces coloaded with $Ru^{II}P^{2+}$ and $Ru^{III}OH_2{}^{3+}$ (or $Ru^{III}OH^{2+}$), back electron transfer to the latter results in the buildup of $-Ru^{II}OH_2{}^{2+}$ away from the initial injection site(s) due to the random diffusion of the injected electron in TiO_2 nanoparticle. Cross-surface electron transfer from $-Ru^{II}OH_2{}^{2+}$ to remote $-Ru^{III}P^{3+}$ occurs on a time scale from hundreds of microseconds to milliseconds. Under steady state photolysis conditions, comparable to the solar photon flux, electron injection, and cross-surface electron transfer led to the buildup of $-Ru^{III}P^{3+}$, $-Ru^{III}OH^{2+}$, and the catalytic precursor for water oxidation, $-Ru^{IV}{=}O^{2+}$.

ASSOCIATED CONTENT

Supporting Information

Electrochemistry, data analysis details, energy and electron transfer results on ZrO_2. This material is available free of charge via the Internet at http://pubs.acs.org.

AUTHOR INFORMATION

Corresponding Author

tjmeyer@unc.edu

Present Address

‡A.I.: Division of Molecular Materials Science, Graduate School of Science, Osaka City University 3-3-138 Sugimoto, Sumiyoshi-ku, Osaka 558−8585, Japan.

Author Contributions

†W.S. and A.I. contributed equally.

Notes

The authors declare no competing financial interest.

ACKNOWLEDGMENTS

This work was partially funded by the UNC Energy Frontier Research Center (EFRC): Center for Solar Fuels, an EFRC funded by the U.S. Department of Energy, Office of Science, Office of Basic Energy Sciences, under Award DE-SC0001011, supporting K.H., R.A.B., J.J.C., and M.K.B. W.S. was supported by the CCHF, an EFRC funded by the U.S. Department of Energy, Office of Science, Office of Basic Energy Sciences, under Award Number DE-SC0001298at the University of Virginia. A.I. was supported by U.S. Department of Energy, Office of Science, Office of Basic Energy Sciences, under Award Number DE-FG02-06ER15788. H.L. is supported by a Royster Society Fellowship. We acknowledge support for the purchase of instrumentation from the UNC EFRC: Center for Solar Fuels, funded by the U.S. Department of Energy, Office of Science, Office of Basic Energy Sciences under award number DE-SC0001011, and by UNC SERC ("Solar Energy Research Center Instrumentation Facility") funded by the U.S. Department of Energy, Office of Energy Efficiency & Renewable Energy under award number DE-EE0003188. The authors wish to thank Dr. Byron Farnum for help on spectra modeling.

REFERENCES

(1) Barber, J. *Chem. Soc. Rev.* **2009**, *38*, 185.
(2) Barber, J.; Andersson, B. *Nature* **1994**, *370*, 31.
(3) Alstrum-Acevedo, J. H.; Brennaman, M. K.; Meyer, T. J. *Inorg. Chem.* **2005**, *44*, 6802.
(4) Morris, A. J.; Meyer, G. J.; Fujita, E. *Acc. Chem. Res.* **2009**, *42*, 1983.
(5) Swierk, J. R.; Mallouk, T. E. *Chem. Soc. Rev.* **2013**, *42*, 2357.
(6) Hambourger, M.; Moore, G. F.; Kramer, D. M.; Gust, D.; Moore, A. L.; Moore, T. A. *Chem. Soc. Rev.* **2009**, *38*, 25.
(7) Song, W.; Chen, Z.; Brennaman, M. K.; Concepcion, J. J.; Patrocinio, A. O. T.; Murakami Iha, N. Y.; Meyer, T. J. *Pure Appl. Chem.* **2011**, *83*, 749.
(8) Karlsson, S.; Boixel, J.; Pellegrin, Y.; Blart, E.; Becker, H.-C.; Odobel, F.; Hammarström, L. *J. Am. Chem. Soc.* **2010**, *132*, 17977..
(9) Song, W.; Glasson, C. R. K.; Luo, H.; Hanson, K.; Brennaman, M. K.; Concepcion, J. J.; Meyer, T. J. *J. Phys. Chem. Lett.* **2011**, *2*, 1808.
(10) Ashford, D. L.; Song, W.; Concepcion, J. J.; Glasson, C. R. K.; Brennaman, M. K.; Norris, M. R.; Fang, Z.; Templeton, J. L.; Meyer, T. J. *J. Am. Chem. Soc.* **2012**, *134*, 19189.
(11) Hanson, K.; Torelli, D. A.; Vannucci, A. K.; Brennaman, M. K.; Luo, H.; Alibabaei, L.; Song, W.; Ashford, D. L.; Norris, M. R.; Glasson, C. R. K.; Concepcion, J. J.; Meyer, T. J. *Angew. Chem., Int. Ed.* **2012**, *124*, 12954.
(12) Moss, J. A.; Yang, J. C.; Stipkala, J. M.; Wen, X.; Bignozzi, C. A.; Meyer, G. J.; Meyer, T. J. *Inorg. Chem.* **2004**, *43*, 1784.
(13) Huynh, M. H. V.; Dattelbaum, D. M.; Meyer, T. J. *Coord. Chem. Rev.* **2005**, *249*, 457.
(14) Sykora, M.; Maxwell, K. A.; DeSimone, J. M.; Meyer, T. J. *Proc. Natl. Acad. Sci.* **2000**, *97*, 7687.
(15) Striplin, D. R.; Reece, S. Y.; McCafferty, D. G.; Wall, C. G.; Friesen, D. A.; Erickson, B. W.; Meyer, T. J. *J. Am. Chem. Soc.* **2004**, *126*, 5282.
(16) Serron, S. A.; Aldridge, W. S.; Fleming, C. N.; Danell, R. M.; Baik, M.-H.; Sykora, M.; Dattelbaum, D. M.; Meyer, T. J. *J. Am. Chem. Soc.* **2004**, *126*, 14506.
(17) Ardo, S.; Meyer, G. J. *J. Am. Chem. Soc.* **2010**, *132*, 9283.
(18) Ardo, S.; Meyer, G. J. *J. Am. Chem. Soc.* **2011**, *133*, 15384.
(19) Gardner, J. M.; Beyler, M.; Karnahl, M.; Tschierlei, S.; Ott, S.; Hammarström, L. *J. Am. Chem. Soc.* **2012**, *134*, 19322.
(20) Hoertz, P. G.; Goldstein, A.; Donley, C.; Meyer, T. J. *J. Phys. Chem. B* **2010**, *114*, 14772.
(21) Trammell, S. A.; Yang, J.; Sykora, M.; Fleming, C. N.; Odobel, F.; Meyer, T. J. *J. Phys. Chem. B* **2001**, *105*, 8895.
(22) Higgins, G. T.; Bergeron, B. V.; Hasselmann, G. M.; Farzad, F.; Meyer, G. J. *J. Phys. Chem. B* **2006**, *110*, 2598.
(23) Magnuson, A.; Anderlund, M.; Johansson, O.; Lindblad, P.; Lomoth, R.; Polivka, T.; Ott, S.; Stensjö, K.; Styring, S.; Sundström, V.; Hammarström, L. *Acc. Chem. Res.* **2009**, *42*, 1899.
(24) Youngblood, W. J.; Lee, S.-H. A.; Kobayashi, Y.; Hernandez-Pagan, E. A.; Hoertz, P. G.; Moore, T. A.; Moore, A. L.; Gust, D.; Mallouk, T. E. *J. Am. Chem. Soc.* **2009**, *131*, 926.
(25) Youngblood, W. J.; Lee, S.-H. A.; Maeda, K.; Mallouk, T. E. *Acc. Chem. Res.* **2009**, *42*, 1966.
(26) Zhao, Y.; Swierk, J. R.; Megiatto, J. D.; Sherman, B.; Youngblood, W. J.; Qin, D.; Lentz, D. M.; Moore, A. L.; Moore, T. A.; Gust, D.; Mallouk, T. E. *Proc. Natl. Acad. Sci. U.S.A.* **2012**, *109*, 15612.
(27) Dismukes, G. C.; Brimblecombe, R.; Felton, G. A. N.; Pryadun, R. S.; Sheats, J. E.; Spiccia, L.; Swiegers, G. F. *Acc. Chem. Res.* **2009**, *42*, 1935.
(28) Brimblecombe, R.; Koo, A.; Dismukes, G. C.; Swiegers, G. F.; Spiccia, L. *J. Am. Chem. Soc.* **2010**, *132*, 2892.
(29) Moore, G. F.; Blakemore, J. D.; Milot, R. L.; Hull, J. F.; Song, H.-e.; Cai, L.; Schmuttenmaer, C. A.; Crabtree, R. H.; Brudvig, G. W. *Energy Environ. Sci.* **2011**, *4*, 2389.
(30) Li, L.; Duan, L.; Xu, Y.; Gorlov, M.; Hagfeldt, A.; Sun, L. *Chem. Commun.* **2010**, *46*, 7307.
(31) Gao, Y.; Ding, X.; Liu, J.; Wang, L.; Lu, Z.; Li, L.; Sun, L. *J. Am. Chem. Soc.* **2013**, *135*, 4219.
(32) Hardin, B. E.; Sellinger, A.; Moehl, T.; Humphry-Baker, R.; Moser, J.-E.; Wang, P.; Zakeeruddin, S. M.; Grätzel, M.; McGehee, M. D. *J. Am. Chem. Soc.* **2011**, *133*, 10662.
(33) Xiang, X.; Fielden, J.; Rodríguez-Córdoba, W.; Huang, Z.; Zhang, N.; Luo, Z.; Musaev, D. G.; Lian, T.; Hill, C. L. *J. Phys. Chem. C* **2012**, *117*, 918.
(34) Karlsson, S.; Boixel, J.; Pellegrin, Y.; Blart, E.; Becker, H.-C.; Odobel, F.; Hammarstrom, L. *Faraday Discuss.* **2012**, *155*, 233.
(35) Debreczeny, M. P.; Svec, W. A.; Wasielewski, M. R. *Science* **1996**, *274*, 584.
(36) Gillaizeau-Gauthier, I.; Odobel, F.; Alebbi, M.; Argazzi, R.; Costa, E.; Bignozzi, C. A.; Qu, P.; Meyer, G. J. *Inorg. Chem.* **2001**, *40*, 6073.
(37) Concepcion, J. J.; Jurss, J. W.; Norris, M. R.; Chen, Z.; Templeton, J. L.; Meyer, T. J. *Inorg. Chem.* **2010**, *49*, 1277.
(38) Lee, S.-H. A.; Abrams, N. M.; Hoertz, P. G.; Barber, G. D.; Halaoui, L. I.; Mallouk, T. E. *J. Phys. Chem. B* **2008**, *112*, 14415.
(39) Wang, Q.; Zakeeruddin, S. M.; Nazeeruddin, M. K.; Humphry-Baker, R.; Grätzel, M. *J. Am. Chem. Soc.* **2006**, *128*, 4446.
(40) Li, X.; Nazeeruddin, M. K.; Thelakkat, M.; Barnes, P. R. F.; Vilar, R.; Durrant, J. R. *Phys. Chem. Chem. Phys.* **2011**, *13*, 1575.
(41) Trammell, S. A.; Meyer, T. J. *J. Phys. Chem. B* **1998**, *103*, 104.
(42) Chen, Z.; Vannucci, A. K.; Concepcion, J. J.; Jurss, J. W.; Meyer, T. J. *Proc. Natl. Acad. Sci. U.S.A.* **2011**, *108*, E1461.
(43) Hanson, K.; Brennaman, M. K.; Ito, A.; Luo, H.; Song, W.; Parker, K. A.; Ghosh, R.; Norris, M. R.; Glasson, C. R. K.; Concepcion, J. J.; Lopez, R.; Meyer, T. J. *J. Phys. Chem. C* **2012**, *116*, 14837.
(44) Chen, Z.; Concepcion, J. J.; Jurss, J. W.; Meyer, T. J. *J. Am. Chem. Soc.* **2009**, *131*, 15580.
(45) Vannucci, A. K.; Hull, J. F.; Chen, Z.; Binstead, R. A.; Concepcion, J. J.; Meyer, T. J. *J. Am. Chem. Soc.* **2012**, *134*, 3972.
(46) Reisner, E.; Powell, D. J.; Cavazza, C.; Fontecilla-Camps, J. C.; Armstrong, F. A. *J. Am. Chem. Soc.* **2009**, *131*, 18457.
(47) Nelson, J.; Haque, S. A.; Klug, D. R.; Durrant, J. R. *Phys. Rev. B* **2001**, *63*, 205321.
(48) Nelson, J.; Chandler, R. E. *Coord. Chem. Rev.* **2004**, *248*, 1181.
(49) Haque, S. A.; Tachibana, Y.; Willis, R. L.; Moser, J. E.; Grätzel, M.; Klug, D. R.; Durrant, J. R. *J. Phys. Chem. B* **1999**, *104*, 538.
(50) Meyer, T. J.; Huynh, M. H. V. *Inorg. Chem.* **2003**, *42*, 8140.
(51) Nelson, J. *Phys. Rev. B* **1999**, *59*, 15374.
(52) Brennaman, M. K.; Patrocinio, A. O. T.; Song, W.; Jurss, J. W.; Concepcion, J. J.; Hoertz, P. G.; Traub, M. C.; Murakami Iha, N. Y.; Meyer, T. J. *ChemSusChem* **2011**, *4*, 216.
(53) Giokas, P.; Miller, S. A.; Hanson, K.; Norris, M. R.; Glasson, C. R. K.; Concepcion, J. J.; Bettis, S. E.; Meyer, T. J.; Moran, A. M. *J. Phys. Chem. C* **2012**, *117*, 812.
(54) Song, W.; Brennaman, M. K.; Concepcion, J. J.; Jurss, J. W.; Hoertz, P. G.; Luo, H.; Chen, C.; Hanson, K.; Meyer, T. J. *J. Phys. Chem. C* **2011**, *115*, 7081.
(55) Lakadamyali, F.; Reynal, A.; Kato, M.; Durrant, J. R.; Reisner, E. *Chem. Eur. J.* **2012**, *18*, 15464.
(56) Grätzel, M. *CATTECH* **1999**, *3*, 4.
(57) O'Regan, B. C.; Durrant, J. R. *Acc. Chem. Res.* **2009**, *42*, 1799.
(58) Concepcion, J. J.; Tsai, M.-K.; Muckerman, J. T.; Meyer, T. J. *J. Am. Chem. Soc.* **2010**, *132*, 1545.